Research Article | Vol. 26, No. 13 | 25 Jun 2018 | OPTICS EXPRESS 16125
Optics EXPRESS

High sensitivity temperature measurement via mask-free hybrid polymer long period fiber grating

BJORN PAULSON,[1,2,6] HOJOONG JUNG,[1,6] JIHYUN HWANG,[1] SEONGJIN HONG,[1] SANGHWA LEE,[3] JUN KI KIM,[2,3,4] AND KYUNGHWAN OH[1,5,6]

[1]*Institute of Physics and Applied Physics, Yonsei University, 50, Yonsei-ro, Seodaemun-gu, Seoul 120–749, South Korea*
[2]*Department of Convergence Medicine, University of Ulsan College of Medicine, 88, Olympic-ro 43-gil, Songpa-gu, Seoul 05505, South Korea*
[3]*Biomedical Engineering Research Center, Asan Medical Center, 88, Olympic-ro 43-gil, Songpa-gu, Seoul 05505, South Korea*
[4]*kim@amc.seoul.kr*
[5]*koh@yonsei.ac.kr*
[6]*These authors contributed equally to this work*

Abstract: Long-period fiber gratings (LPFGs) are useful for environmental sensing under conditions of high corrosiveness and electromagnetic interference. Most LPFGs are fabricated by coherent or high-power UV illumination of an optical fiber under an amplitude mask, resulting in narrow and environmentally-dependent band rejection. We present a hybrid LPFG waveguide fabricated without an amplitude mask through polymer self-assembly under low-power incoherent UV illumination, which demonstrates high-temperature sensitivity in its transmission spectrum compared to LPFG sensors based purely on silica waveguides. A sensitivity of 1.5 nm °C $^{-1}$ is obtained experimentally for attenuation near 1180 nm, and a sensitivity of 4.5 nm °C $^{-1}$ with a low random error was obtained with a composite of attenuation bands. Finite element method simulations and coupling mode theory reveal this to be due to a thermo-optic coefficient one order of magnitude greater than that of fused silica. The device has potential for a simple and inexpensive transmission intensity based temperature sensor consisting of an infrared light source, the LPFG, a bandpass filter, and a photodiode.

OCIS codes: (160.5470) Polymers; (050.2770) Gratings; (280.6780) Temperature; (220.4610) Optical fabrication.

References and links

1. B. Lee, "Review of the present status of optical fiber sensors," Opt. Fiber Technol. **9**(2), 57–79 (2003).
2. S. W. James and R. P. Tatam, "Optical fibre long-period grating sensors: characteristics and application," Meas. Sci. Technol. **14**(5), R49–R61 (2003).
3. V. Bhatia and A. M. Vengsarkar, "Optical fiber long-period grating sensors," Opt. Lett. **21**(9), 692–694 (1996).
4. D. D. Davis, T. K. Gaylord, E. N. Glytsis, S. G. Kosinski, S. C. Mettler, and A. M. Vengsarkar, "Long-period fibre grating fabrication with focused CO2 laser pulses," Electron. Lett. **34**(3), 302–303 (1998).
5. C.-Y. Lin, L. A. Wang, and G.-W. Chern, "Corrugated Long-Period Fiber Gratings as Strain, Torsion, and Bending Sensors," J. Lightwave Technol. **19**(8), 1159–1168 (2001).
6. W. Ha, K. Oh, Y. Jung, J. K. Kim, W. Shin, I.-B. Sohn, D.-K. Ko, and J. Lee, "Fabrication and characterization of a broadband long-period-grating on a hollow optical fiber with femtosecond laser pulses," J. Korean Phys. Soc. **53**(9(6)), 3814–3817 (2008).
7. A. I. Kalachev, D. N. Nikogosyan, and G. Brambilla, "Long-period fiber grating fabrication by high-intensity femtosecond pulses at 211 nm," J. Lightwave Technol. **23**(8), 2568–2578 (2005).
8. A. D. Kersey, M. A. Davis, H. J. Patrick, M. LeBlanc, K. P. Koo, C. G. Askins, M. A. Putnam, and E. J. Friebele, "Fiber grating sensors," J. Lightwave Technol. **15**(8), 1442–1463 (1997).
9. A. Singh, D. Engles, A. Sharma, and M. Singh, "Temperature sensitivity of long period fiber grating in SMF-28 fiber," Opt. - Int. J. Light Electron Opt. **125**(1), 457–460 (2014).
10. Z. Li, H. Y. Tam, L. Xu, and Q. Zhang, "Fabrication of long-period gratings in poly(methyl methacrylate-co-methyl vinyl ketone-co-benzyl methacrylate)-core polymer optical fiber by use of a mercury lamp," Opt. Lett. **30**(10), 1117–1119 (2005).

#327410 https://doi.org/10.1364/OE.26.016125
Journal © 2018 Received 4 Apr 2018; revised 28 May 2018; accepted 29 May 2018; published 11 Jun 2018

Optics EXPRESS

11. M.-S. Kwon and S.-Y. Shin, "Tunable polymer waveguide notch filter using a thermooptic long-period grating," IEEE Photonics Technol. Lett. **17**(1), 145–147 (2005).
12. L. H. Chen, C. C. Chan, and J. Sun, *High resolution long-period grating temperature sensor* (ACM Press, 2008), pp. 1–4.
13. S. Yin, K.-W. Chung, and X. Zhu, "A novel all-optic tunable long-period grating using a unique double-cladding layer," Opt. Commun. **196**(1-6), 181–186 (2001).
14. S. Khaliq, S. W. James, and R. P. Tatam, "Enhanced sensitivity fibre optic long period grating temperature sensor," Meas. Sci. Technol. **13**(5), 792–795 (2002).
15. H. Jung, Y. G. Seo, W. Ha, D.-K. Kim, S. H. Park, and K. Oh, "Mask-free hybrid long-period fiber grating fabrication by self-assembled periodic polymerization in silica hollow optical fiber," Opt. Lett. **34**(18), 2745–2747 (2009).
16. X. Shu, L. Zhang, and I. Bennion, "Sensitivity characteristics of long-period fiber gratings," J. Lightwave Technol. **20**(2), 255–266 (2002).
17. X. Shu, T. Allsop, B. Gwandu, L. Zhang, and I. Bennion, "High-temperature sensitivity of long-period gratings in B-Ge codoped fiber," IEEE Photonics Technol. Lett. **13**(8), 818–820 (2001).
18. S. W. James, S. Khaliq, and R. P. Tatam, "Enhanced sensitivity fibre optic long period grating temperature sensor," in *2002 15th Optical Fiber Sensors Conference Technical Digest. OFS 2002(Cat. No.02EX533)* (IEEE, 2002), Vol. **1**, pp. 139–142.
19. D. Kowal, G. Statkiewicz-Barabach, P. Mergo, and W. Urbanczyk, "Microstructured polymer optical fiber for long period gratings fabrication using an ultraviolet laser beam," Opt. Lett. **39**(8), 2242–2245 (2014).
20. D.-J. Kim, J.-U. Shin, Y.-T. Han, S.-H. Park, Y.-J. Park, H.-K. Sung, and D.-K. Kim, "Thermal Behavior of Arrayed-Waveguide Grating Made of Silica/Polymer Hybrid Waveguide," ETRI J. **26**(6), 661–664 (2004).
21. J. W. Fleming, "Dispersion in GeO_2–SiO_2 glasses," Appl. Opt. **23**(24), 4486–4493 (1984).
22. B. J. Frey, D. B. Leviton, and T. J. Madison, "Temperature-dependent refractive index of silicon and germanium," in *Optomechanical Technologies for Astronomy* (International Society for Optics and Photonics, 2006), Vol. **6273**, p. 62732J.
23. S. T. Gulati and J. D. Helfinstine, "Fatigue Behavior of GeO2-SiO2 Glasses," MRS Proc. **531**, 133 (1998).
24. D. B. Leviton and B. J. Frey, "Temperature-dependent absolute refractive index measurements of synthetic fused silica," in *Proc. SPIE*, E. Atad-Ettedgui, J. Antebi, and D. Lemke, (2006), Vol. **6273**, p. 62732K.
25. J. M. Jewell, "Thermooptic Coefficients of Some Standard Reference Material Glasses," J. Am. Ceram. Soc. **74**(7), 1689–1691 (1991).
26. T. Erdogan, "Cladding-mode resonances in short- and long-period fiber grating filters," J. Opt. Soc. Am. A **14**(8), 1760–1773 (1997).
27. T. Erdogan, "Cladding-mode resonances in short- and long-period fiber grating filters: errata," J. Opt. Soc. Am. A **17**(11), 2113 (2000).
28. S. Lee, J. Park, Y. Jeong, H. Jung, and K. Oh, "Guided Wave Analysis of Hollow Optical Fiber for Mode-Coupling Device Applications," J. Lightwave Technol. **27**(22), 4919–4926 (2009).
29. K. Oh, S. Choi, Y. Jung, and J. W. Lee, "Novel hollow optical fibers and their applications in photonic devices for optical communications," J. Lightwave Technol. **23**(2), 524–532 (2005).
30. R. Mittra and, J. R. Pace, "Generalized scattering matrix analysis of waveguide discontinuity problems," in *Quasi-Optics XIV* (Polytechnic Inst. Brooklyn, 1964).
31. G. W. Chern and L. A. Wang, "Transfer-matrix method based on perturbation expansion for periodic and quasi-periodic binary long-period gratings," J. Opt. Soc. Am. A **16**(11), 2675 (1999).
32. R. Kashyap, *Fiber Bragg Gratings* (Academic, 2009).
33. T. W. MacDougall, S. Pilevar, C. W. Haggans, and M. A. Jackson, "Generalized expression for the growth of long period gratings," IEEE Photonics Technol. Lett. **10**(10), 1449–1451 (1998).
34. F. Shen, C. Wang, Z. Sun, K. Zhou, L. Zhang, and X. Shu, "Small-period long-period fiber grating with improved refractive index sensitivity and dual-parameter sensing ability," Opt. Lett. **42**(2), 199–202 (2017).
35. F. Shen, K. Zhou, N. Gordon, L. Zhang, and X. Shu, "Compact eccentric long period grating with improved sensitivity in low refractive index region," Opt. Express **25**(14), 15729–15736 (2017).
36. P. Wang, H. Zhao, G. Brambilla, G. Farrell, and L. Yuan, "Long period grating inscribed in multimode fibre interferometer and its application in refractive index sensing," in *Proc. SPIE*, H. J. Kalinowski, J. L. Fabris, and W. J. Bock, (2015), Vol. **9634**, p. 96346A.

1. Introduction

Optical sensing devices are commonly used in small and lightweight form-factors for the detection of temperature, strain, and pressure where resistance to corrosion and resistance to electromagnetic interference are of high priority [1]. Long-period fiber gratings (LPFGs) have found numerous applications in these optical sensors and devices, due to their narrow and environmentally-dependent band rejection [2]. The band attenuation behavior of LPFGs results from a periodic index modulation along the fiber core which enables coupling between the fundamental core mode and the cladding modes at specific, resonant frequencies. The band attenuation can be perturbed by environmentally-induced changes in the waveguide

Optics EXPRESS

dispersion and grating period, resulting in high sensitivity to temperature and mechanical strain.

Many techniques are available for fabrication of periodic gratings in fiber. Aside from techniques for the instantiation of temporary gratings based on pressure, twisting, and strain, techniques for the permanent formation of static gratings based on the photosensitivity of the GeO_2–SiO_2 fiber core have a long history [3] and are common in industrial applications, but require either an amplitude mask or high power ultraviolet lasers [3,4]. Many other techniques exist for static grating formation based on cladding corrugation [5,6] and point-by-point manufacturing [7], among others, but typical temperature sensitivity for silica devices operating in the near infrared remains low, between 13 and 150 pm $°C^{-1}$ [3,8,9]. Techniques for the formation of plastic gratings [10,11] generally require more sophisticated fabrication methods.

While the typical device sensitivity to temperature and strain for solid state devices remains low [3,8,9], LPFGs incorporating narrow claddings with liquid materials for increased cladding mode overlap have achieved performances of 2 to 4 nm $°C^{-1}$ [12,13], while LPFG temperature sensors incorporating specialty core materials as well as index-matching oil claddings have achieved sensitivities of nearly 20 nm $°C^{-1}$ [14]. In both of these cases, sensitivity performance has come at the cost of increased device toxicity, fabrication complexity, and device fragility.

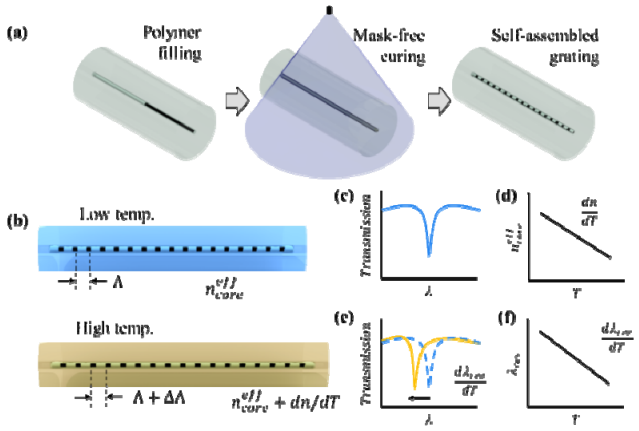

Fig. 1. Grating fabrication and device concept. (a) Fabrication of the self-assembled fiber grating is mask-free and low power. (b) Temperature change results in changes in the core refractive index and grating pitch. (c) The periodic grating results in attenuation at a specific wavelength band. (d) The core refractive index changes with temperature, (e) resulting in shifting of the main attenuation band, (f) the band shift is linear in temperature.

In a previous publication [15], the authors have reported an alternative to previous fiber gratings by proposing a hybrid structure: a polymer core in a silica hollow optical fiber (HOF) that, after a mask-free curing process with a low-power incoherent UV lamp, forms a self-assembled periodic polymer structure which behaves as a long period grating. The previously published device is entirely solid state, with a principal period of 15 μm, and a sharp, strong attenuation band near 1190 nm. Temperature sensitivity of the device has not been published; however, it was suspected that temperature sensitivity would be high due to the large thermo-optic coefficient of the cured polymer core.

Here is reported, for the first time to the best knowledge of the authors, the high temperature sensitivity of a solid-state LPFG sensor based on a self-assembled periodic polymer structure. The LPFG was fabricated following the previous work [15], with a low-power mask-free method using incoherent UV light. Coupled-mode simulations reveal that coupling is to the 10^{th}-order mode, and that the high sensitivity is due to the high thermo-optic

Optics EXPRESS

coefficient of the polymer. High sensitivity is obtained experimentally, with 1.5 nm °C^{-1} shift for a resonance band at 1180 nm, with higher shifts for bands at higher wavelengths, which allow formation of a high-sensitivity and low random error composite metric. Application of the device in a low-cost temperature sensor is simulated, revealing potential for the device in future thermal sensing applications.

2. Device fabrication and experimental setup

Long period gratings were formed via a mask-free self-assembly process, as described in previous work [15], and shown schematically in Fig. 1. A step-index silica hollow optical fiber (HOF) with a central hole diameter of 6 microns and a central GeO_2-doped ring of thickness 2.3 microns was filled to a length of 5 cm with a fluorinated acrylate UV-curable epoxy (ChemOptics Exguide ZPU13-RI 450) via capillary action. The resultant continuously polymer-filled capillary was cured under a low-power incoherent UV lamp in a two-step process, first at 1 mW cm^{-2} for 1 min to initialize the self-assembly and set the grating pitch, and then at 10 mW cm^{-2} for 10 min to fully cure the polymeric structure. The combined effects of solidification and viscosity mismatch in the phase transition result in self-assembled periodic structures composed of periodically alternating solid polymer plugs and gas-containing spaces. Control of period was achieved by manual selection of devices, resulting in limited device repeatability. Following polishing to a 5 mm length, the grating pitch varied from 15 to 18 microns, with 17 microns being the grating pitch over the majority of the device, as shown in Fig. 2. Devices were fabricated using mechanical splicers to immobilize and couple single-mode fibers (SMF) to both polished, polymer-filled end faces of the LPFG-filled HOF. By minimizing core mode mismatch between LPFG and SMF, total splicing losses of about 5 dB per facet were obtained. Devices were immobilized by polymer epoxy in a mechanical splicer, resulting in highly stable splices and high strain resistance of the device as a whole.

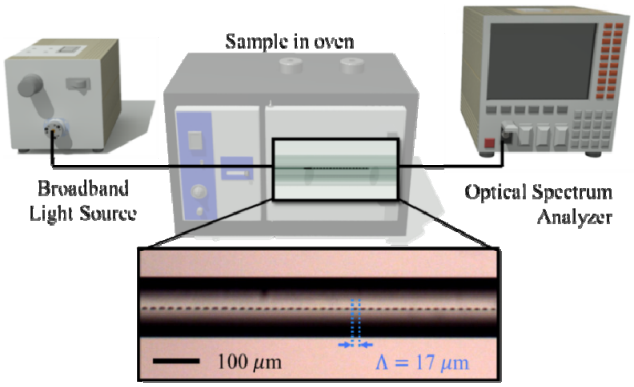

Fig. 2. Setup of the experiment, with device micrograph.

To investigate the thermal response of the polymer LPFGs in transmission, self-assembled polymer LPFGs were spliced mechanically to single-mode optical fiber (SMF) and transmission spectra were measured while the LPFG was driven through a precisely-controlled temperature range, as shown in schematic in Fig. 2. The environmental temperature accuracy was ± 0.1 °C. To allow the oven to equalize in temperature, 3~5 minutes were allowed between measurements at different temperatures. A temperature range from 10 to 70 degrees was verified experimentally. As the resonances are very sensitive to temperature and change too much to track clearly over a wide temperature range, only the spectral changes over a temperature range of 25 to 28.5 degrees are shown in this paper.

Optics EXPRESS

3. Experimental results

3.1 Principle attenuation band

In agreement with prior results, a principle attenuation band was observed around 1186 nm at 25 °C showing a narrow and strong resonance, with a coupling strength of 6 dB at the center of the peak and a FWHM of 24 nm, as shown in Fig. 3(a). The thermal behavior of the principle attenuation band is shown in Fig. 3(b).

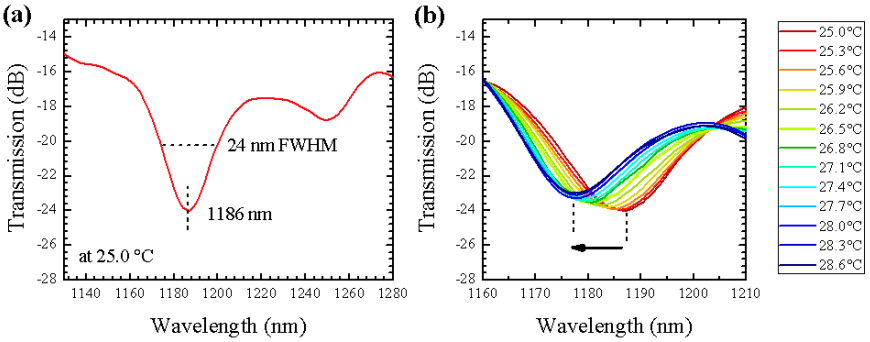

Fig. 3. (a) Main attenuation band of the grating at the reference temperature of 25 °C. (b) Variation of transmission spectrum and specific attenuation peaks on a small temperature range from 25~28.6 °C demonstrates thermal behavior of the attenuation band.

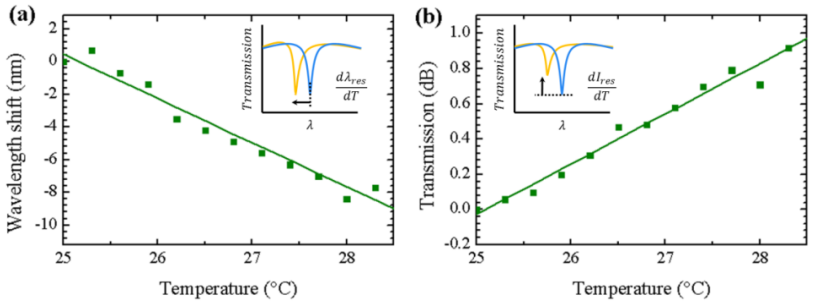

Fig. 4. (a) Attenuation band wavelength shift and (b) transmission shifts in the principal attenuation peak on the temperature range from 25~28.6 °C shows linear shifting behavior with device sensitivity of −1.5 nm °C^{-1} near 1180 nm.

Device sensitivity to temperature was characterized and is shown in Figs. 4(a) and 4(b), in which device sensitivity is presented by plotting the attenuation band wavelength shift and attenuation amplitude shift of the peak, respectively, as functions of temperature from 25 to 28.6 °C. In keeping with the theory of LPFGs (to be discussed in the next section), the wavelength shifts are linear, with residuals approximately as expected due to limitations in temperature control and grating non-uniformity. A linear change in attenuation peak transmission was observed, likely due to the relatively small range of temperature measurement.

3.2 Secondary attenuation bands

Weaker additional bands (which are larger than the multimode interference threshold) appear around 1240 nm, 1370 nm, and 1460 nm, indicating either weak coupling to additional grating periods or interference between the fundamental and additional modal coupling from the secondary modes. These bands showed strongly thermally-dependent transmission behavior, with weak attenuation at 25 degrees and higher attenuation at higher temperatures.

Optics EXPRESS

The additional attenuation bands and their thermal behavior are shown in Figs. 5 and 6. The band near 1370 nm was not included in the analysis, since it shows bifurcating double-band behavior at higher temperatures. Such behavior has been previously observed for modes in LPFGs, and is indicative of coupling to modes near the limit of sensitivity [16].

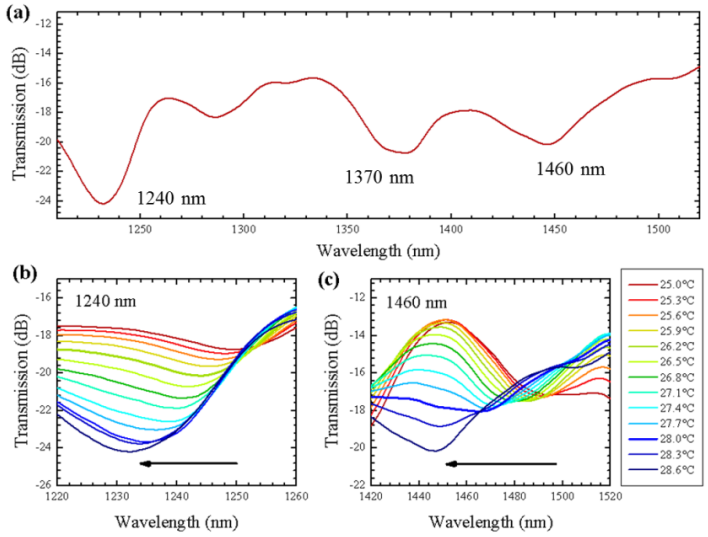

Fig. 5. (a) Transmission spectrum of the LPFG shows secondary attenuation bands near 1240 nm, 1370 nm, and 1460 nm for 26°C. (b) Thermal behavior of the 1240 nm attenuation band and (c) of the 1460 nm band show high temperature sensitivity.

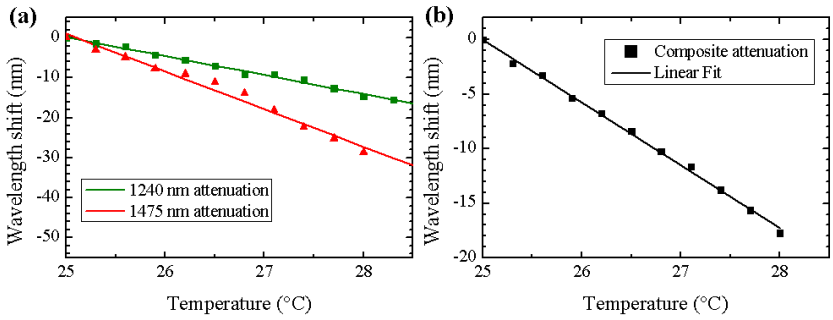

Fig. 6. (a) Attenuation band shifts in the secondary attenuation peaks on the temperature range from 25~28.6 °C show nearly linear shifting behavior with increasing device sensitivity at higher wavelengths. (b) Composite attenuation shift function attains repeatable and monotonic shifting behavior with 4 nm °C^{-1} sensitivity.

In order to decrease the random error of the temperature measurement, a composite shift was created by taking the mean of the shifts in the 1180, 1240, and 1460 nm attenuation bands, and is shown in Fig. 6(b). The composite attenuation shows higher temperature accuracy than any of the individual shifts, and has a sensitivity of –4.48 ± 0.09 nm °C^{-1}. The sensitivity of the present device compares favorably to previous high-sensitivity LPFG temperature sensors using B-Ge co-doped fiber [17], which demonstrated a maximum of –2.75 nm °C^{-1} over 10 degrees, and displays higher temperature shift linearity than oil-based sensing devices [18].

Optics EXPRESS

4. Theory and discussion

4.1 Grating quality

The dominant period along the self-assembled grating was 15~18 microns. Transmission spectra, as shown in Fig. 3(a) and 5(a), show a strong attenuation band at 1186 nm, with 6 dB attenuation and 24 nm FWHM, as well as weaker attenuation bands around 1240 nm, 1370 nm, and 1460 nm, with similar or lower FWHM, but less attenuation. The observed attenuation is greater than that observed in other simple polymer LPFG devices, while the FWHM is significantly larger [10], although in comparison to more recent polymer LPFG devices, the resonant coupling attenuation and FWHM of the hybrid device are both significantly smaller [19]. This wide FWHM is indicative of a slight grating non-periodicity, which occurs as a result of the self-annealing process, and may also be due to the multimodal core simulated in the next section.

Table 1. Refractive indices and thermo-optic coefficients of the hybrid LPFG waveguide

		1180 nm, 25 °C	1200 nm, 25 °C			Ref.
Region	Material	n	n	dn/dT (°C^{-1})	α (ppm °C^{-1})	
Core	Polymer	1.452486	1.452376	−0.000187	300~400	[20]
Gas pocket	Air	1	1	0		
Ring	4.5% GeO_2	1.455044	1.454804	0.000009	0.9	[21–23]
Cladding	Fused silica	1.448319	1.448092	0.000008	9.8	[24,25]

4.2 Transverse modes

The resonance attenuation behavior of LPFGs arises as the periodic index perturbation induces coupling between the core modes and the forward-propagating cladding modes of the polymer-filled HOF. The periodic effective index modulation is a result of the microbubble air structures in the polymer-filled HOF, which depress the effective mode index. The coupling is highly dependent on the modal overlap and phase matching between the transverse guiding modes of the LPFG core and cladding [26,27]. While modes can be calculated for simple structures using analytical methods, for the asymmetric gas pocket-containing core of the hybrid polymer LPFG, finite element method (FEM) simulation is a more adaptable method of calculating the transverse modes.

The transverse guiding modes and propagation constants of the LPFG were calculated using FEM simulation for the core, ring, and cladding modes, using the software COMSOL. Simulations followed analytical boundary conditions and mesh geometries previously used for HOF [28]. Refractive indices and thermo-optic behavior were modelled as in Table 1, with full thermo-optic behavior modelled for the silica cladding [24], and the GeO_2-doped ring [21,22], while the polymer core was modeled with the measured linear thermo-optic coefficient [20]. The Germania doping ratio of the HOF ring was assumed 4.5 mol. % in a step-index geometry [29]. Thermal expansion of the cross-section was calculated to be less than 1 nm, which is less than the mesh size, and so was not included in modal simulations.

Although the refractive index of the polymer core is lower than that of the Germania-doped ring, the polymer core was shown in FEM simulations to support the majority of the energy for the identified HE_{11} fundamental mode, as well as guided $TE_{01,}$ $TM_{01,}$ and HE_{21} for a total of six modes in this wavelength range. The cladding supports approximately 105 cladding modes of the form $HE_{l,m}$ for azimuthal order l = 1, in addition to modes of higher azimuthal order. Figure 7 shows the HE_{11} fundamental mode of the microbubble-containing ring core and the polymer-filled ring core which define the grating, as well as the $HE_{1,3}$ and $HE_{1,10}$ cladding modes for the asymmetric geometry.

Optics EXPRESS

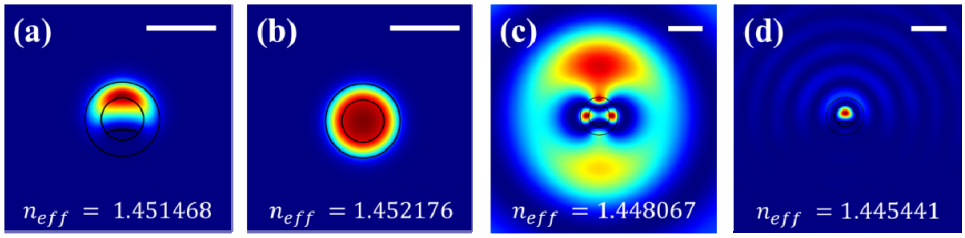

Fig. 7. Select transverse modes of the polymer waveguide at 25 °C for the polynomial-filled cross section at a wavelength of 1180 nm. (a) HE_{11} fundamental mode of the gas pocket-containing core. b) HE_{11} fundamental mode of the polymer-filled core (c) $HE_{1,3}$ cladding mode and (d) $HE_{1,10}$ cladding modes couple differently to the core mode. Scale bars are 10 microns.

4.3 Modal overlap and modal modulation depth

In order to determine the range of modes responsible for grating formation, as well as the grating effective modulation depth, coupling was examined between the gas pocket-containing geometry's guided modes and the modes of the filled polymer geometry. For modes accessible to FEM, significant coupling was only observed to occur between the fundamental $HE_{1,1}$ mode as shown in Fig. 7(a) and $HE_{1,m}$ modes. The effective indices of the filled polymer $HE_{1,m}$ modes are shown in Table 2 for m = 1 to 11. Significant modal overlap only occurs for the m = 1 mode shown in Fig. 7(b). This establishes an effective grating with a modulation depth δn of 0.000708 at 1180 nm.

Table 2. Coupling modes for grating formation with modulation depths

	1200 nm, 25 °C			1200 nm, 28 °C	
Mode	Coupling coefficient c	n_{eff}	Modal Mod. depth δn	n_{eff}	Modal Mod. depth δn
$HE_{1,1}$ void	—	1.451468	0	1.4513270	0
$HE_{1,1}$ core	0.532	1.452176	–0.000708	1.451982	–0.000655
$HE_{1,2}$ core	0.008	1.448176	0.003293	1.448200	0.003127
$HE_{1,3}$ core	0.016	1.448074	0.003394	1.448096	0.003231
$HE_{1,4}$ core	0.023	1.447904	0.003563	1.447922	0.003404
$HE_{1,5}$ core	0.029	1.447670	0.003798	1.447682	0.003645
$HE_{1,6}$ core	0.033	1.447375	0.004092	1.447378	0.003949
$HE_{1,7}$ core	0.034	1.447024	0.004444	1.447017	0.004310
$HE_{1,8}$ core	0.032	1.446617	0.004851	1.446600	0.004726
$HE_{1,9}$ core	0.002	1.446148	0.005320	1.446129	0.005198
$HE_{1,10}$ core	0.023	1.445609	0.005859	1.445597	0.005730
$HE_{1,11}$ core	0.009	1.445016	0.006452	1.444991	0.006336

4.4 Modal coupling and coupled mode theory

Separate from the modal modulation depth, the difference in material refractive index forms a refractive index difference $\Delta n(x, y)$ across the fiber cross section. In the hybrid self-assembled grating, this refractive index difference is largest in the gas pockets, which are off-center and comprise roughly 15% of the polymer core's cross-sectional area. In these regions, the refractive index difference results in a perturbation of ~0.452486 at 1180 nm and 25 °C. Because the gas pocket spaces are filled with gas at approximately atmospheric pressure, while the polymer has a refractive index near that of doped silica, the index difference in the cladding modes would be accurately treated using the scattering matrix method [30] or the transfer matrix method [31]. Here operation of the hybrid LPFG is described qualitatively using coupled mode perturbation theory, using the gas pocket-containing cladding modes as a basis. It should be noted that coupling between the otherwise orthogonal guided transverse modes in typical fiber gratings is made possible by asymmetric modulation of the grating across the fiber transverse cross-section. In typical LPFGs, inscription asymmetry arises as a

Optics EXPRESS

result of the absorptive nature of the fiber photochemistry, with the core area nearer the illumination source expressing the highest refractive index modulation [32].

In the hybrid LPFG, asymmetry occurs mainly as a result of the gas pockets being off-center in the fiber. The coupling between core-guided mode and cladding-guided mode is given by the cross-coupling coefficient [32]:

$$\kappa_{ac} = \frac{\omega\varepsilon_0}{4}\int_{-\infty}^{+\infty} 2n\Delta n(x,y)\vec{E}_{core}(x,y)\cdot\vec{E}^*_{clad}(x,y)dA, \tag{1}$$

where $\Delta n(x,y)$ is the refractive index perturbation of 0.452486 mentioned above, $\vec{E}_{core}$ and $\vec{E}_{clad}$ are the electric fields of the transverse core and cladding modes, respectively, as calculated by FEM, and n is the core refractive index of 1.452486 at 1180 nm and 25 °C. Cross-coupling coefficients for $HE_{1,m}$ modes in the void geometry are shown in Fig. 8, and reveal several modes with strong coupling. Interestingly, there is a qualitative difference between the core behavior of the low-order cladding modes m = 2 to m = 6 and m>10, as modes with m < 6 do not allow the existence of a strong electric field in the polymer core, as shown in Fig. 7(c), while modes with m>9 allow the existence of a stable Gaussian-like mode inside the polymer core, as shown in Fig. 7(d). Both strong cross-coupling and self-coupling are necessary for a mode to exhibit coupled attenuation behavior in the grating device.

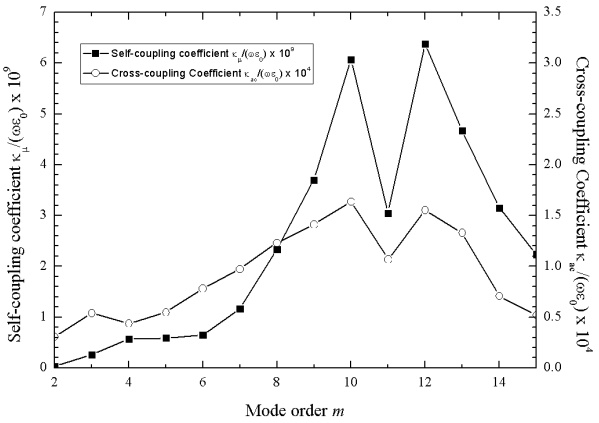

Fig. 8. Self-coupling coefficients and cross-coupling coefficients for the $HE_{1,m}$ modes of the hybrid LPFG.

Through application of the phase matching condition [26,27], resonant wavelengths λ_{res} in the coupled mode model are given by [5]

$$\lambda_{res} = \frac{(n^{eff}_{core} - n^{eff}_{clad})\Lambda}{1+(\kappa_{clad} - \kappa_{core})\Lambda/2\pi} \tag{2}$$

where Λ is the grating pitch, n^{eff}_{core} is the effective index of the core transverse mode, n^{eff}_{clad} is the effective index of the cladding mode, and

$$\kappa_{\mu} = \frac{\omega\varepsilon_0}{4}\int_{-\infty}^{+\infty} 2n\Delta n(x,y)\vec{E}_{\mu}(x,y)\cdot\vec{E}^*_{\mu}(x,y)dA \tag{3}$$

is the self-coupling coefficient, identical to the cross-coupling coefficient of a mode with itself. The self-coupling coefficients and cross-coupling coefficients with the fundamental mode are shown for the modes of the gas pocket-containing core in Fig. 8.

Optics EXPRESS

4.5 Attenuation bands

From Eqs. (1) and (2) can be calculated the predicted attenuation wavelengths of each mode. These attenuation bands are shown in Table 3.

Table 3. Predicted attenuation bands for the hybrid LPFG waveguide

	25 °C		25 °C
Coupled mode	λ_{res} (nm)	Coupled mode	λ_{res} (nm)
$HE_{1,8}$	1286	$HE_{1,12}$	1057
$HE_{1,9}$	1235	$HE_{1,13}$	1236
$HE_{1,10}$	1141	$HE_{1,14}$	1314
$HE_{1,11}$	1282	$HE_{1,15}$	1360

From this model only the m = 10 mode is strongly coupled to the fundamental mode of the waveguide near 1180 nm, with predicted attenuation at 1141 nm. A further strong peak is predicted outside of the measurement range, while weaker peaks are predicted in the 1240~1280 nm region. This qualitatively describes the observed experimental results, despite significant deviation which is likely due to the limited applicability of coupled mode approximations to this system. The m = 10 attenuation band corresponds to effective index differences of 0.0058 refractive index units between coupled core and cladding modes at 25 °C, and a corresponding difference in self-coupling coefficient of -2.69×10^{-5}.

4.6 Temperature sensitivity

Thermal variation in LPFGs results in shifting and modulation of the grating attenuation bands. Following Eq. (2), the overall shift in the spectral location of a resonance band is a function of the fiber properties, the grating period, and the order of the coupled cladding modes. For systems in which the shift in the core refractive index is much larger than that in the most shifted cladding mode, and for which the refractive index shift is nearly linear, Shu *et al.* have introduced a simplified expression [33,16] for the temperature shift in terms of dispersive properties of the fiber. For the hybrid LPFG, this expression is modified to include the denominator of Eq. (2):

$$\frac{d\lambda_{res}}{dT} = \gamma(\alpha + \Gamma_{temp})\lambda_{res} + \frac{\left[\alpha(\kappa_{core} - \kappa_{clad}) + \frac{d\kappa_{core}}{dT} - \frac{d\kappa_{clad}}{dT}\right]\frac{\lambda_{res}}{2\pi}}{1/\Lambda + \frac{(\kappa_{clad} - \kappa_{core})}{2\pi}}. \quad (4)$$

Here Γ_{temp} is the thermal sensitivity coefficient, which describes the sensitivity of each mode as a function of temperature, and is defined in Eq. (5). The value α is the coefficient of thermal expansion of the waveguide, and $\gamma = (n_{core}^{eff} - n_{clad}^{eff,m})/(n_{core}^{g} - n_{clad}^{g,m})$ quantifies the contribution of the waveguide dispersion to the sensitivity for group refractive indices n^g. The calculated parameters γ and Γ_{temp} for the first 15 $HE_{1,m}$ cladding modes are shown in Fig. 9 (a), while thermal shifts are shown in Fig. 9(b).

The thermal sensitivity coefficient Γ_{temp} is defined by

$$\Gamma_{temp} = \frac{\xi_{core} n_{core}^{eff} - \xi_{clad} n_{clad,m}^{eff}}{n_{core}^{eff} - n_{clad,m}^{eff}}, \quad (5)$$

where ξ_{core} and ξ_{clad} denote the thermo-optic coefficients of the core and cladding materials, respectively [16]. For the polymer core of the hybrid LPFG, $\xi_{core} = -1.87 \times 10^{-4}$ °C^{-1}, while $\xi_{clad} = 8 \times 10^{-6}$ °C^{-1} [24]. Due to the high thermo-optic coefficient of the core, the thermal

Optics EXPRESS

sensitivity coefficient is found to be –0.0748, about 140 times higher than that for a high-sensitivity B-Ge co-doped LPFG [17] previously reported.

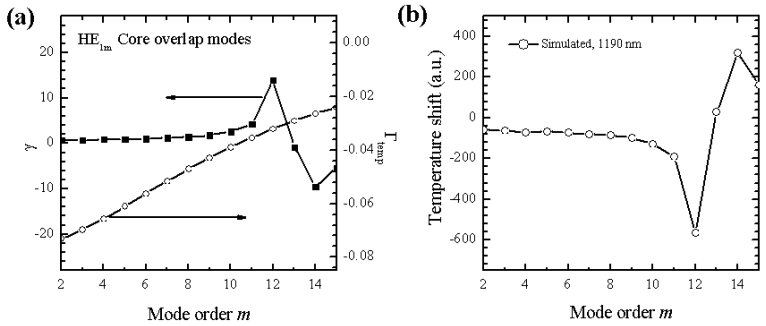

Fig. 9. (a) General sensitivity coefficient γ for the $HE_{1,m}$ modes and temperature sensitivity coefficient Γ_{temp} for the $HE_{1,m}$ modes. (b) Simulated temperature shift for the $HE_{1,m}$ modes at 1186 nm from the core and ring mode on the observed temperature range 25~28.6 °C.

The experimentally measured attenuation bands in the transmission spectra are observed to show nearly linear temperature response, in agreement with theory. In Fig. 4(a), the temperature sensitivity of the primary attenuation band is shown to be −1.5 nm °C^{-1}, while for the secondary resonance peaks at 1240 and 1460 nm in Fig. 6, it is shown to be −4.7 ± 0.1 and −9.4 ± 0.4 nm °C^{-1}, respectively. This is comparable to the sensitivity of −2.75 nm °C^{-1} previously observed in B-GeO_2 co-doped LFPGs [17]. The temperature sensitivity is observed to be negative, in agreement with the simulated effective index difference shown in Fig. 9(b).

The observed blueshift of the attenuation band with temperature is due to the fiber geometry, to the optical properties of the waveguide materials, to thermal expansion of the grating period, and to change in the coupling coefficients with temperature, as quantified in Eqs. (4) and (5). Of these, the most significant was found to be the thermal sensitivity coefficient Γ_{temp}, which takes a value of about −0.04 in the observed modal range, in comparison to the grating thermal expansion α, which is limited by expansion of the ZPU13-450 polymer to about 300~400 ppm [20], and thus contributes negligibly to the thermal sensitivity of this device, despite being several orders of magnitude greater than that of silica. Thus the high thermal sensitivity comes as a result of the high thermo-optic coefficient of the polymer core material, as well as the high core power fraction of the cladding modes. The product $\gamma \cdot \Gamma_{temp}$ takes very large values between −0.003 and 0.01 for the first eleven modes, resulting in expected temperature shifts significantly larger than observed. This likely reflects the limitations to the coupled mode theory for high modulation gratings [5].

In addition to wavelength shifts based on temperature, transmission shifts were also observed. The power coupled from the core mode into the cladding mode is a function of the squared sine of the coupling constant, the detuning parameter, and the grating length, all of which change with temperature [2]. Along the small temperature measurement range in this experiment, we found the temperature shift to be linear over the measured range, with a slope of 0.28 ± 0.01 dB °C^{-1}. The secondary attenuation peaks show strongly temperature-modulated attenuation behavior, which is likely related to either a strong temperature dependence of the coupling coefficients, or temperature dependence in the modal cutoff wavelength.

The spectrum of the present device differs significantly from those of previously published long period grating sensors of similar period [34,35], which is most likely due to

Optics EXPRESS

effects of the multimodal core, but may also be related to limitations of the coupled mode approximation, non-periodicities in duty cycle, core size, and limited grating chirping. Multimodality and chirping may be expected to result in broadening and decrease in extinction ratio of the attenuation bands, and may also contribute to limited multimode interference. Our full spectrum resembles that of an LPFG inscribed in a multimodal fiber previously [36]. This highly attenuated behavior, as well as the interaction between multimodality, and the various nonperiodicities, are being studied by the authors for a future publication.

Although the analyzed temperature range of the thermal sensor is quite small, the devices are promising for application to high-sensitivity temperature measurement where the temperature range is known and low cost optical sensing with ease of fabrication is prioritized.

4.7 Low-cost sensor simulation

With a wide FWHM, the hybrid LPFG is ideal for the creation of bandpass filtered sensors. In the interest of fabricating a low-cost, high-sensitivity optical transmission sensor with a single photodiode (PD), simulations were carried out to calculate the optical attenuation due to the present LPFG in series with commercially available laser diodes and bandpass filters. This simple design would allow optical determination of temperature with a single photodiode and an infrared light source rather than a full optical spectrum analyzer (OSA). Changes in the transmission intensity with temperature were simulated for PD sensors using QDLaser DFB laser diode (LD) QLA1161-88A0 and for LD QFLD-1231-350S, as well for as a generic LED with Thorlabs bandpass filter FB1450-12. These sensors have center wavelengths 1188, 1231, and 1450 nm, respectively, and FWHM of 0.5, 10, and 12 nm. The resultant transmission sensitivities are shown in Fig. 10, and demonstrate average sensitivities of 0.97, –1.98, and –1.77 dB $°C^{-1}$, respectively. For the DFB-LD based sensor, the transmission (black line) is found to follow the observed thermal transmission spectrum of the LPFG fiber device (blue dashed line) directly, due to the narrow bandwidth, while there is a small but noticeable variance between the two in the LD and filtered LED sensors. The thermal attenuation of the LPFG at the center wavelength is the inverse of the blue dashed lines in Fig. 10. The results show a potential "off-band" application of the LPFG in low cost semiconductor PD-based temperature sensors, which is enabled by its large temperature shift and wide FWHM.

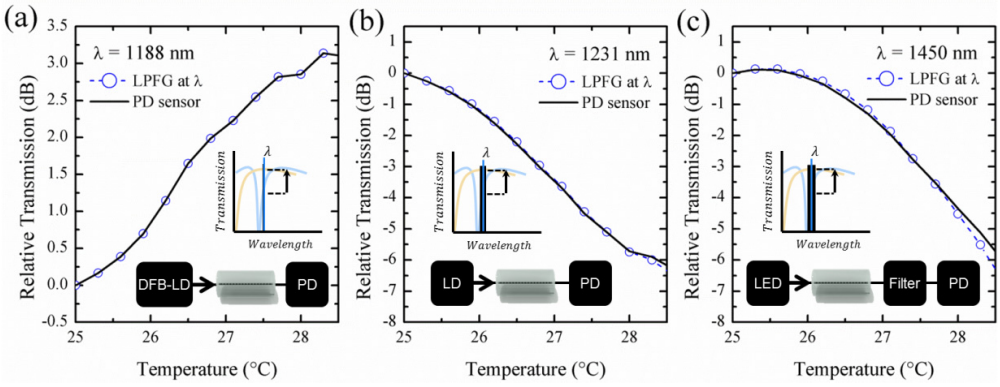

Fig. 10. Expected temperature sensitivities for simple temperature sensors based on an infrared light source, the hybrid polymer LPFG, a bandpass filter, and a semiconductor photodiode. (Blue dashes) measured transmission of the SMF-LPFG-SMF at the fixed sensor center wavelength. (Solid lines) expected transmission signal of the photodiode-based sensor. (Insets) Schema depicting the measurement and sensor function relative to the grating attenuation. Expected transmission from (a) a commercially available DFB LD at 1188 nm, (b) an IR LD with 10 nm FWHM at 1231 nm, (c) a generic IR LED with bandpass filter at 1450 nm.

Optics EXPRESS

5. Conclusion

We report the temperature sensitivity of a long period fiber grating fabricated with low UV power and without an amplitude mask. We examined the device experimentally and performed coupling mode simulation of the sensitivity of the LPFG. The strongest attenuation bands appear near 1180 and 1250 nm, and have high temperature sensitivities of −1.5 and −4.7 nm °C^{-1}, while the weaker 1460 nm attenuation band had temperature sensitivity of −9.4 nm °C^{-1}, respectively. With a composite wavelength shift, random error was reduced, and a sensitivity of −4.48 nm °C^{-1} was obtained. The observed sensitivities are several orders of magnitude larger than those of LPFGs fabricated from photosensitive germanium-silica optical fibers, and are comparable with those of B-Ge co-doped optical fibers. The observed sensitivity can be explained by the high thermo-optic coefficient of the polymer core. The resulting hybrid LPFG is promising as a low-cost solid-state temperature sensor of high sensitivity.

Funding

Ministry of Science, ICT & Future Planning (IITP 2014-044-014-002, NRF-2012M3A7B4049800, BSRP 2016k1A3A1A09918616); Agency for Defense Development of Korea (UD160069BD); National Research Foundation of Korea Basic Science Research Program (2014R1A1A2057773, 2015K2A7A1035896); Ministry of Trade, Industry & Energy Industrial Technology Innovation Program (10080726).

Acknowledgments

The authors would like to thank Dr. Marzieh Pournoury for helpful discussions during the development of the manuscript. The authors declare that there are no conflicts of interest related to this article.